Available online at www.sciencedirect.com
SCIENCE DIRECT®
Journal of the Mechanics and Physics of solids
53 (2005) 1223–1247
JOURNAL OF THE MECHANICS AND PHYSICS OF SOLIDS
www.elsevier.com/locate/jmps

Stochastic simulation of dislocation glide in tantalum and Ta-based alloys

C.S. Deo[a,b,*], D.J. Srolovitz[a], W. Cai[c], V.V. Bulatov[c]

[a]*Princeton Materials Institute & Department of Mechanical and Aerospace Engineering, Princeton University, Princeton, NJ 08544, USA*
[b]*Department of Materials Science and Engineering, University of Michigan, Ann Arbor, MI 48109, USA*
[c]*Chemistry and Materials Science Directorate, Lawrence Livermore National Laboratory, Livermore, CA 94550, USA*

Received 19 October 2004; received in revised form 4 January 2005; accepted 11 January 2005

Abstract

We employ a kinetic Monte Carlo algorithm to simulate the motion of *a* $1/2\langle 1\,1\,1\rangle$-oriented screw dislocation on a $\{0\,1\,1\}$-slip plane in body centered cubic Ta and Ta-based alloys. The dislocation moves by the kink model: double kink nucleation, kink migration and kink–kink annihilation. Rates of these unit processes are parameterized based upon existing first principles data. Both short-range (solute–dislocation core) and long-range (elastic misfit) interactions between the dislocation and solute are considered in the simulations. Simulations are performed to determine dislocation velocity as a function of stress, temperature, solute concentration, solute misfit and solute–core interaction strength. The dislocation velocity is shown to be controlled by the rate of nucleation of double kinks and the dependence of the double kink nucleation rate on stress and temperature are consistent with existing analytical predictions. In alloys, dislocation velocity depends on both the short- and long-range solute dislocation interactions as well as on the solute concentration. The short-range solute–core interactions are shown to dominate the effects of alloying on dislocation mobility. The present simulation method provides the critical link between atomistic calculations of fundamental

*Corresponding author. Los Alamos National Laboratory, MST-8, P.O. Box 1663, MS G755, Los Alamos 87544, USA. Tel.: +1 505 667 1755; fax: +1 505 667 8021.
E-mail address: cdeo@lanl.gov (C.S. Deo).

0022-5096/$ - see front matter
doi:10.1016/j.jmps.2005.01.003

dislocation and solute properties and large scale dislocation dynamics that typically employ empirical equations of motion.

1. Introduction

Dislocations are the primary carriers of crystal plasticity in metals. Dislocation motion is driven by externally applied stresses and resisted by intrinsic or extrinsic obstacles. The dominant intrinsic barriers are associated with the lattice resistance (Peierls barriers), while extrinsic barriers include solute, second phase particles and other dislocations. The Peierls formulation assigns an energy to each dislocation segment that depends on its location with respect to its position on the glide plane. The lattice resistance for the motion of screw dislocations in body centered cubic (bcc) metals such as tantalum is very high compared to the resistance to the motion of edge dislocations. Hirsch et al. (1957, 1960) and Hirsch (1959) proposed that the large Peierls stress for screw dislocation motion in bcc crystals is attributable to a the extension of the dislocation core. Several subsequent studies (Basinski et al., 1970; Duesbery, 1983a,b; Duesbery and Vitek, 1998; Vitek and Taylor, 1974; Vitek, 1976, 1985) have shown that the core of the screw segments relaxes into low-energy non-planar configurations. This introduces deep valleys in the Peierls energy function that is aligned along the burgers vector and possesses the periodicity of the lattice. At low temperatures, dislocations tend to adopt low energy configurations and consequently the dislocation population predominantly consists of long screw segments. In order to move a segment normal to itself, the dislocation core must first be constricted and hence the attendant Peierls stress is large. This results in a much higher barrier for screw dislocation motion than for edge dislocations and suggests that the rate limiting mechanism for plastic deformation in bcc metals is the motion of screw dislocations.

Atomistic simulations (Ismail-Beigi and Arias, 2000; Rao and Woodward, 2001; Wang et al. (2001); Woodward and Rao, 2001; Yang and Moriarty, 2001; Yang et al., 2001a,b) have shed some light onto the properties of dislocation cores and short-range dislocation segment–segment interactions, such as the energies of a single isolated kinks on a dislocation and the associated Peierls stress for kink motion. These studies confirm the earlier picture regarding the extended nature of the screw dislocation in bcc tantalum. Dislocation dynamics (DD) simulations (Bulatov et al. 1998, 2001; Tang et al., 1998, 1999) attempt to link dislocation properties and the resulting mechanical behavior of crystals by tracking the motion of a large number of dislocations. They incorporate atomistic information as parameters in empirical relations for dislocation mobility. Such a description replaces the true kink dynamics of a dislocation with a mean field measure of the average mobility of a dislocation line. Ortiz and co-workers (Cuitino and Ortiz, 1993; Ortiz, 1999; Stainier et al., 2003) performed studies of crystal plasticity using phase field methods to define a dislocation loop and employing universality classes to determine the onset of yielding.

Kinetic Monte Carlo (kMC) simulations can be used to provide a more realistic link between kink dynamics and the averaged dynamics of a dislocation line. In this manner, kMC simulations can be viewed as the link between atomistic and DD simulations. kMC simulations use atomistic results for the nature of the core energetics, short-range dislocation segment interactions, and rate theory to compute dislocation velocities as a function of stress and temperature. Several researchers have performed kMC studies of dislocation behavior to investigate the relationship between dislocation mobility and factors such as external stress and temperature. Lin and Chrzan (1999) developed a kMC model that describes the stress and temperature dependence of dislocation velocity on the applied stress and temperature of an idealized dislocation. Cai et al. (1999) performed kMC simulations of a pair of partial dislocations in silicon and the interaction and coupling between the dissociated partials in the presence of external stress in a thermal environment. In both approaches, the dislocation was represented as a system of pure edge and screw segments constrained to move on its glide plane. Stresses on the dislocation included contributions from the dislocation self-stress, calculated by considering the elastic interactions of the segments with each other. The dislocations were assumed to move by the kink mechanism through adjacent Peierls valleys, via nucleation of double kinks on the dislocation and lateral kink migration and annihilation. Cai et al. (2001, 2002) developed a similar kMC model for studying dislocation motion in molybdenum, where the dislocation (again discretized as a set of screw and edge segments) was allowed to cross-slip onto secondary glide planes, creating vacancy loops and clusters.

We recently developed a new kMC model (Deo et al., 2005) that extends the earlier work on dislocation mobility by applying a first passage time Markov chain analysis to rare events. In addition to studying dislocation mobility using the kink mechanism in a pure crystal, we were able to incorporate the effects of solute atoms that interact with the dislocation and, hence, modify the dislocation motion. Such a model is readily applicable to the study of dislocation motion in real alloys, where the dislocation moves through adjacent Peierls valleys by the kink mechanism and the solute interacts with the dislocation through short-range solute–core interactions and through long-range elastic fields. Results from atomistic simulations can be incorporated in the development of Peierls energy functions and dislocation–solute interactions. In such applications, the kMC simulation procedures can predict the dependence of the dislocation mobility on such parameters as stress, solute concentration, solute type and solute diffusivity. The results can then be used to make DD simulations responsive to questions associated with how alloying modifies plastic deformation. The procedure replaces arbitrary assumptions about the nature of dislocation mobility with input based upon microscopic understanding.

In the present paper, we apply our kMC model of dislocation migration to the special case of the motion of screw dislocations in bcc Ta and its alloys. In particular, we examine screw dislocation velocity in Ta as a function of stress and temperature based upon atomistic input. We then consider how substitutional solutes affect screw dislocation mobility in Ta as a function of these same parameters.

2. Simulation model

We focus on the case of an $(a/2)[1\,\bar{1}\,1]$ screw dislocation on the $(1\,1\,0)$ glide plane in bcc Ta.

While the dislocation has, on average, a screw orientation, it consists of screw and edge dislocation segments such that kinks on the screw dislocation are perfect edge segments. This model does not allow for cross-slip of the screw segments or climb of the edge segments. The dislocation is assumed to move via a kink mechanism—this involves the nucleation of pairs of kinks of opposite sign, kink migration and the mutual annihilation of oppositely signed kinks (see Fig. 1). The kMC simulation samples different classes of possible kink nucleation and migration events. Kink–kink annihilation is considered as a special case of kink migration.

Fig. 2 shows a representation of the simulation cell as a 3-d simple cubic lattice. The $\{1\,1\,0\}$ glide plane has normal $\hat{y}$ (at position $y=0$) and the $\vec{b} = a_0/2[1\,\bar{1}\,1]$ Burgers vector is along the z-direction. The atomic spacing in the z-direction is $b=\sqrt{3}a_0/2$, the spacing in the x-direction is $h=a_0/\sqrt{6}$ and the spacing between the $\{1\,1\,0\}$ glide planes is $l=a_0/\sqrt{2}$. The glide plane (at position $y=0$) is discretized in the form of a square grid. At each grid point i, with co-ordinates $(x_i,0,z_i)$, an order parameter $\phi(x_i,0,z_i)$ is defined to identify the location of the dislocation:

$$\phi(x_i,0,z_i)=\begin{cases}1, & (x_i,0,z_i) \text{ is a slipped region of the glide plane,}\\ 0, & (x_i,0,z_i) \text{ is an unslipped region of the glide plane.}\end{cases} \tag{1}$$

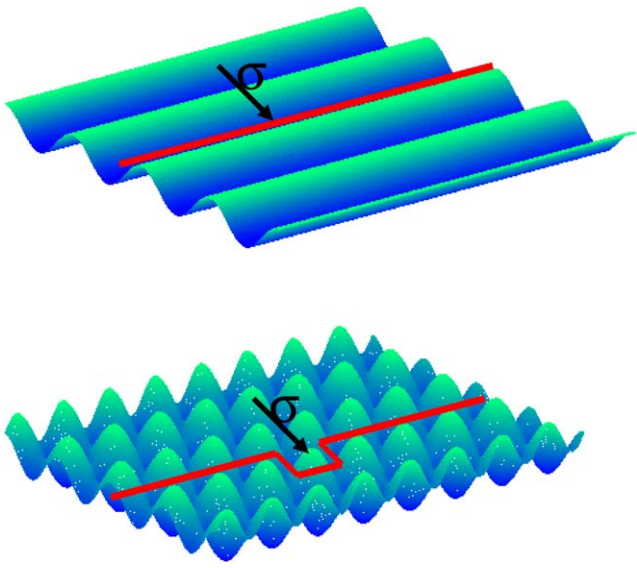

Fig. 1. A schematic illustration of the energy landscape with and without large secondary Peierls barriers. As the kinks migrate along the dislocation line, they may encounter additional barriers to migration.

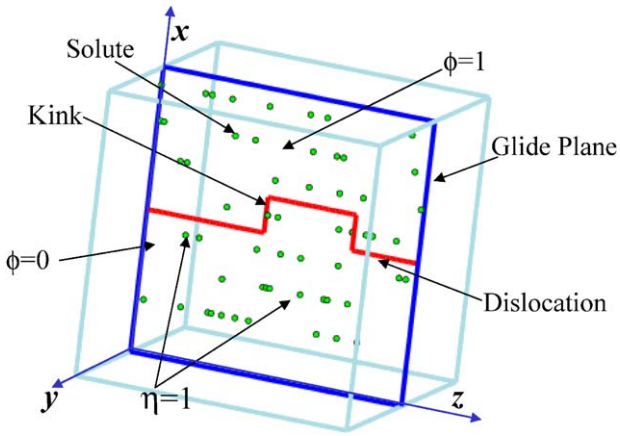

Fig. 2. An illustration of the dislocation–solute model. The order parameter $\phi(x_i, 0, z_i)$ is defined over the glide plane and is used to identify the location of the dislocation. The solute atoms are distributed in three dimensions and are represented by a field $\eta(x_i, y_i, z_i)$ (see text for details).

A dislocation line segment lies between any pair of nearest neighbor (square) lattice points in the glide plane that have different values of ϕ. The model can easily be extended to a system of multiple dislocations by allowing the order parameter to take additional values.

Elastic theory for kink formation and diffusion as a mechanism for dislocation motion was first developed by Eshelby (1962), Seeger and Sestak (1971) and Seeger (1981), and has been reviewed in detail by Hirth and Lothe (1982). Kinks nucleate in oppositely signed pairs. Following Hirth and Lothe (1982), the nucleation rate for a double kink of width $1b$ (where b is the Burgers vector) is,

$$j_{\mathrm{dk}} = \omega \exp\left(-\frac{2E_{\mathrm{k}} - \tau_{\mathrm{eff}} b^2 h/2}{k_{\mathrm{B}} T}\right), \tag{2}$$

where ω is the frequency with which double kinks attempt to form, E_{k} the energy of an isolated kink, h is the kink height, $k_{\mathrm{B}}T$ is the thermal energy, and τ_{eff} is the local resolved stress that includes the applied stress, the stress field of the solutes and the self-stress due to elastic interactions between the dislocation elements. The term $2E_{\mathrm{k}} - \tau_{\mathrm{eff}} b^2 h/2$ can be viewed as the activation enthalpy for double kink nucleation. Hirth and Lothe (1982) estimate the double kink nucleation energy as a function of the dislocation width w to be

$$F(w) = 2F_{\mathrm{k}} - \frac{\mu b^2 h^2}{8\pi w}\left(\frac{1+\nu}{1-\nu}\right) - \sigma b h w, \tag{3}$$

where the nominal orientation of the dislocation line is along the Burgers vector, μ is the shear modulus, ν the Poisson's ratio and σ the applied stress. Since the elastic interactions between the nucleating kinks are included in the calculation of σ_{eff}, the

two expressions are equivalent at a kink–kink separation of $1b$. The energy of two well separated kinks $2E_k$ is a parameter in the model and can be obtained from first principles calculations. In the case of Ta, Yang and co-workers (2001, 2001a,b) have calculated this value to be 0.96 eV using modified pseudopotentials. When the nucleation site for a double kink is at a solute position, it experiences a local energy barrier that depends on the solute–core interaction, characterized by an energy parameter E_b that is added to the activation enthalpy for double kink nucleation.

In the absence of an obstacle, kinks on the screw dislocation in Ta have very high mobilities, limited predominantly by lattice damping (drag) resistance, characterized by the coefficient B_k (Yang and Moriarty, 2001). In such a case, the kink velocity v_k is proportional to the driving force experienced by the kink (Nadgornyi, 1988):

$$v_k = \frac{\tau_{eff}}{B_k} b. \tag{4}$$

Kinks require thermal activation to overcome the local energy barrier associated with solute atoms near the core. The rate of kink migration is determined by the magnitude of the solute–kink interaction energy E_b. The velocity with which a kink bypasses a solute along its path is

$$v_k = \frac{\tau_{eff} bh}{k_B T} \omega a^2 \exp\left(-\frac{E_b - \tau_{eff} b^2 h/2}{k_B T}\right), \tag{5}$$

where a is the jump distance ($a = b$) and the attempt frequency ω is of the order of the Debye frequency. Therefore, we describe the motion of kinks using Eq. (4) at all times other than when the kink encounters a solute, in which case we employ Eq. (5).

The stress field τ_{eff} contains contributions from the external applied stress σ^A, from all of the dislocation segments (i.e., the self-stress), and the long-range stress field associated with solute atoms:

$$\tau_{eff} = \sigma^A + \sigma^{solute} + \sigma^{self\text{-}stress}. \tag{6}$$

The self stress, $\sigma^{self\text{-}stress}$, is the stress exerted on a dislocation segment by all other dislocation segments and is calculated as proposed by Hirth and Lothe (1982) (i.e., as a sum of the stress fields, at the point of interest, associated with each of the straight line dislocation segments). For a general segmented dislocation configuration, the stresses from the individual line segments can be transformed as tensors to a common co-ordinate system and summed to give the total self-stress at a point. Details of the calculation of the self stress may be found elsewhere (Cai et al., 1999; Deo et al., 2005; Hirth and Lothe, 1982). In all cases, the effective stress field τ_{eff} is computed at the mid-point of each dislocation segment.

The substitutional solute atoms are distributed in three dimensions and are represented by a field $\eta(x_i, y_i, z_i)$ which is one at lattice points occupied by solute atoms and zero at lattice points occupied by solvent (Ta) atoms. We divide the solute–dislocation interaction into two parts depending on the distance $|r|$ of the solute from the dislocation segment (see Fig. 3); one associated with the long-range

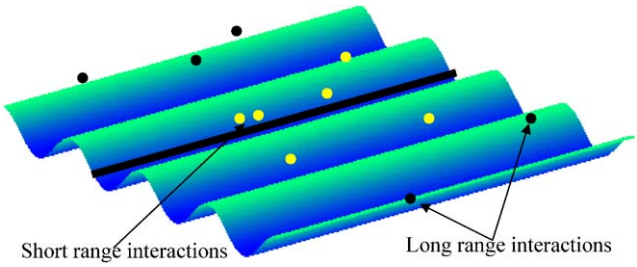

Fig. 3. A schematic illustration of dislocation motion in alloys—in addition to the energy landscape, the dislocation is also affected by the presence of solute particles. Light particles are in the glide plane, dark particles are out of the glide plane.

elastic fields of the solute and the other with the short-range solute–core interaction. If $r = |\vec{r}| > \sqrt{2}a_0$, the stress field is calculated as

$$\sigma_{\theta\theta} = \sigma_{\phi\phi} = \frac{\mu}{2\pi}\frac{\delta v}{r^3} = \frac{-\sigma_{rr}}{2}. \tag{7}$$

This is the stress field associated with a point source of dilatation of magnitude $\delta v = (3/a)(\mathrm{d}a/\mathrm{d}C_s)$, where a is the lattice parameter in the alloy with solute fraction C_s (Haasen, 1979, 1983). If the solute is within $\sqrt{2}a$ of the dislocation core, the stress field of the solute is assumed to be zero and it is replaced with a solute–core interaction energy. This avoids the singularity in Eq. (7) as r tends to zero. We assume that such a core–solute interaction provides a barrier E_b to the motion of the kink (see Eq. (5)).

Of the unit processes in the kink diffusion model, nucleation of kink pairs is the slowest and, hence, plays an important role in determining both the velocity of the dislocation and the efficiency of the kMC simulation. If a double kink is formed with a width smaller than a critical width, the two kinks attract and quickly self-annihilate. The rates of formation and self-annihilation events are so fast that the simulation would normally waste most of its time forming and annihilating sub-critical double kinks. Such a problem was encountered in earlier simulations of dislocation motion (Cai et al., 2002). A solution to this problem lies in nucleating a double kink of finite width w_0 which is greater than the critical width w^*, such that the double kink, once formed, is stable and embryonic nucleation events never occur. In order to overcome the double kink formation/annihilation bottleneck, we treat it as a 1-d random walker in double kink width space. The distribution of times for the formation of a double kink of width w is obtained by applying an exact first passage time analysis to the 1-d random walk as modeled by a temporally homogenous discrete state Markov process (Gillespie, 1992). Details of this method can be found elsewhere (Deo and Srolovitz, 2002). The critical double kink width is also affected by solutes that interact directly with the dislocation core through the modification of the energy landscape (i.e., the solutes modify the barriers for kink motion). This effect is also incorporated in the consolidated nucleation rate using the first passage time analysis. Describing nucleation of double kinks in regions with solute using the

Markov chain approach accelerates the simulations by a factor of approximately 10^4 (in the present simulations) over simply waiting for a supercritical double kink to form from embryonic double kinks.

We implemented the kMC model using the N-fold way (or BKL) method (Bortz et al,, 1975), which uses a variable time increment to incorporate events that occur on widely different time scales. A similar procedure was employed by Cai et al. to simulate dislocation motion in pure Mo (Cai et al., 2001) and Si (Cai et al., 1999) and by Scarle et al. (2001) to study dislocation motion in silicon. The kMC model is described in detail in another paper (Deo et al., 2005) with application to the motion of a screw dislocation in Mo-based alloys.

In the kMC simulations, one event occurs during each step. This event is chosen based upon a sampling of all possible events that could occur, weighted by their rates (in the units of s^{-1}). These events include nucleation of double kinks and the displacement of the individual kinks. The double kink nucleation rates (j_{dk}) are calculated from the application of the first passage time analysis (Deo and Srolovitz, 2002) and Eq. (2) taking into account the local solute environment. Kink velocities are calculated using Eq. (4) or Eq. (5) depending on the absence or presence of a solute in the path of the kink, respectively. Kink annihilation events are treated as special cases of kink migration and are parameterized by the same set of equations (Eqs. (4) and (5)).

Each step of the kMC procedure involves updating ϕ over the glide plane to reflect double kink nucleation, kink migration or kink–kink annihilation as per (Deo et al., 2005). The variable time increment is sampled from the exponential distribution of all rate dependent events. The procedure is repeated at each kMC step. The mean dislocation position is calculated as the mean x-position of all of the dislocation segments over the glide plane (located based upon the field ϕ). The dislocation velocity is computed as the local slope of the mean dislocation position versus time. In Section 2.1, we examine the dependence of the dislocation velocity of $a\langle 1\,1\,1\rangle$ oriented screw dislocation in Ta on temperature, stress, and interactions with solutes.

2.1. *Motion of a* $\langle 1\,1\,1\rangle$*-oriented screw dislocation in pure Tantalum*

Computer simulations (Duesbery et al., 1973; Duesbery and Vitek, 1998; Vitek and Taylor, 1974; Vitek, 1976, 1985) and experimental studies (Hirsch et al., 1957, 1960; Hirsch, 1959) studies of the core of the $(a/2)[1\,\bar{1}\,1]$ screw dislocation in bcc Ta have suggested that a 3-d extension of the core of the dislocation leads to deep valleys in the Peierls energy functional and consequently a high Peierls stress. The screw dislocation in Mo has a much higher Peierls stress and hence a much smaller mobility than the edge dislocation. The screw dislocation moves by the nucleation of pairs of edge character kinks which migrate in a direction transverse to the line direction of the dislocation and meet and annihilate with opposite character kinks. While atomistic studies have suggested several different types of kinks (Bulatov et al., 1997; Duesbery, 1983a,b) with unique mobilities, a lack of reliable data on the energetics of the motion of the kinks compels us to assume that all of the kinks have the same diffusivity.

The mobility of the screw dislocation in Ta is small because the nucleation rate of double kinks of a size greater than the critical width is small. Although we have replaced the real double kink nucleation events that would normally be seen in standard kMC simulations with the supercritical nucleation events predicted from the Markov chain analysis, the detailed shape of the dislocation line are statistically equivalent to those found using standard kMC, provided we look on time scales that are long compared with those for single supercritical nucleation events. Thus, introduction of the Markov chain approach has no impact on measured dislocation velocity, but a profound impact on the time required to execute the simulations.

Fig. 4 shows the variation of the dislocation velocity (v_D) with the length of the dislocation (z-dimension of the simulation cell), L. These results show that the dislocation velocity increases with system size L and then asymptotes to an L-independent value at large system size. This size dependence has two origins. When the size of the simulation cell is small, the elastic interaction between a kink and its image across the periodic cell boundary is important. When the dislocation line length is small compared with the thermal equilibrium spacing between kinks, kinks annihilate preferentially on their double kink nucleation mate, rather than on other kinks. Clearly, the simulation cell size required to overcome this limitation is function of temperature and stress. Increasing temperature and/or increasing stress lead to larger equilibrium kink concentrations, as suggested by the form of Eq. (2). The simulation results shown below were all obtained using simulation cell lengths of sufficient size to ensure that the dislocation velocity is independent of system size.

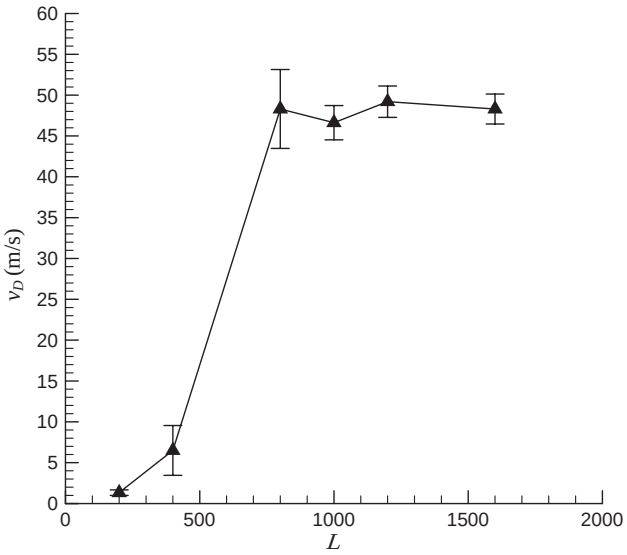

Fig. 4. A plot of the screw dislocation velocity in Ta as a function of system size (lengths of screw dislocation L for the same set of operational parameters. The results are independent of system size at higher system sizes.

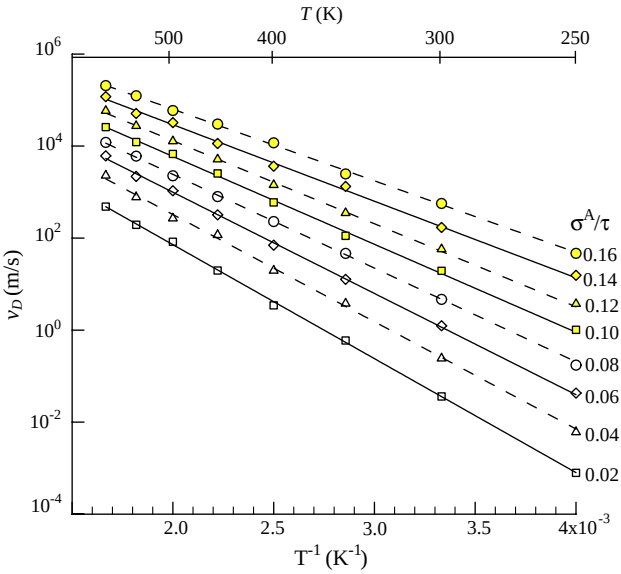

Fig. 5. A semi-log plot of the dislocation velocity v_D as a function of the inverse temperature for eight different stress values for pure Ta. The corresponding temperature is shown in the bar above the plot. The applied stress is expressed as a fraction of the Peierls stress τ_P.

Fig. 5 shows the logarithm of the $(a/2)[1\,\bar{1}\,1]$ screw dislocation velocity v_D as a function of the inverse temperature in pure Ta for several values of the applied stress (σ^A) in the range $0.02 \leqslant \sigma^A/\tau_P \leqslant 0.16$ or $2 \times 10^{-4} \leqslant \sigma^A/\mu \leqslant 1.6 \times 10^{-3}$. (Larger values of the applied stress were not used in order to ensure the validity of the kink model description of dislocation migration (Hirth and Lothe, 1982).) The data for each applied stress appears to be linear, implying that the dislocation velocity is well described by the Arrhenius form

$$v_D = A \exp\left(-\frac{Q}{k_B T}\right). \tag{8}$$

The activation energy Q and the pre-exponential factor A data are tabulated in Table 1 and the variation of Q with applied stress is shown in Fig. 6a. These data suggest that both A and Q are each linear functions of the applied stress;

$$A^{Ta} = \alpha_1^{Ta} + \alpha_2^{Ta}\sigma/\tau_P = [0.52_{(\pm 0.26)} + 40_{(\pm 8.5)}\sigma/\tau_P] \times 10^7\ \mathrm{m/s},$$
$$Q^{Ta} = \beta_1^{Ta} + \beta_2^{Ta}\sigma/\tau_P = [0.49_{(\pm 0.06)} - 1.22_{(\pm 0.12)}\sigma/\tau_P]\,\mathrm{eV}.$$

In the analytical model for the dislocation velocity suggested by Hirth and Lothe (1982), the activation energy for the dislocation velocity is $Q = E_k$ for an infinitely long dislocation ($E_k = 0.48$ eV in the present simulations). In that analytical model (Hirth and Lothe, 1982), the effective activation energy Q of the glide velocity is equal to E_k for segments long enough so that kink lifetimes are limited by kink–kink

Table 1
The constants in the Arrhenius velocity–temperature relation as a function of applied stress (Eq. (8), Fig. 5)

σ^A/τ_P	Q (eV)	$A \times 10^7$ (m/s)
0.02	0.48	0.78
0.04	0.45	1.6
0.06	0.44	3.4
0.08	0.42	2.6
0.10	0.41	4.4
0.12	0.40	4.2
0.14	0.37	5.8
0.16	0.35	6.7

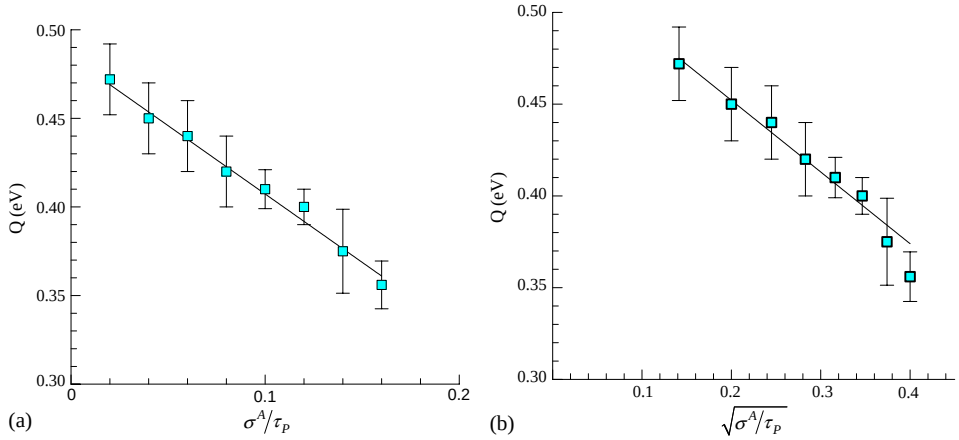

Fig. 6. (a) The activation energy Q plotted as a function of the stress (expressed as a fraction of the Peierls stress τ_P). (b) The activation energy Q plotted as a function of square root of the stress (expressed as a fraction of the Peierls stress τ_P).

annihilation, and $Q = 2E_k$ for segments short enough for kink pairs to sweep out the whole segment. Since the simulation results clearly show that the activation energy is a linear function of the applied stress, this model cannot adequately describe the simulation data. However, it can be modified to include the effect of stress. In the kMC simulation, we are attempting to model an infinite dislocation through periodic boundary conditions with each periodic cell containing more than a single kink pair. Thus we can assume that the kink lifetimes are limited by kink–kink annihilation. Hence, if the rate of dislocation motion is controlled by double kink nucleation, the activation energy for dislocation motion (parameter Q in Eq. (8)) will be half of that for double kink nucleation, i.e., half the maximum value of the energy from Eq. (3):

$$Q = \frac{1}{2}\left[2E_k - \frac{\sigma bhw^*}{2}\right], \tag{9}$$

where w^* is the critical half-loop width. The constant term in the activation energy of Eq. (9) is consistent with that found from our simulations (from a linear fit to the data in Fig. 6a, i.e., $E_k = 0.48\,\text{eV}$. Our previously reported simulations of screw dislocation motion in Mo support this observation (i.e., that the activation energy for the dislocation velocity is equal to E_k in the zero stress limit (Deo et al., 2005)). Hirth and Lothe (1982) suggest that the critical half-loop width is inversely proportional to the square root of the stress (i.e., the width that maximizes Eq. (3),

$$w^* = \left(\frac{\mu b h}{8\pi\sigma}\right)^{1/2}. \tag{10}$$

This suggests that the activation energy should scale as a constant minus a term proportional to the square root of stress. Although the activation energy found in the simulation appears to scale linearly with the applied stress (Fig. 6a), Fig. 6b shows that it is almost as well fit by the form $Q = \alpha - \beta\sqrt{\sigma}$, where $\alpha_{\text{simul}} = 0.54\,\text{eV}$ and $\beta_{\text{simul}} = 0.39\,\text{eV}/\sqrt{\tau_P}$. Eqs. (9) and (10) provide a theoretical estimate of $\beta = (\mu b^3 h^3/8\pi)^{1/2}$. If we choose the same values of the constants as used in the simulation, we find $\beta_{\text{theory}} \approx 0.12\,\text{eV}/\sqrt{\tau_P}$. The simulation and theoretical estimates for α differ by a factor of 1.1 and the β values differ by a factor of 3.2. Given the statistical uncertainty in the simulation data, we conclude that the activation energy for the dislocation velocity in Ta is equal to half of that for the nucleation of a double kink. Further, the theoretical estimate for this quantity is consistent with the analysis of our simulation data. Another possible source for the small disagreement between simulation and the theoretical estimate based upon double kink nucleation may be attributable to the presence of multiple, interacting kinks on the dislocation line (a feature that the double kink nucleation assumption neglects).

Analysis of the anelastic creep measurements for Ta in the limit of zero stress near room temperature (Mizubayashi et al., 1995) suggest the activation enthalpy for kink pair formation (H_{KPF}) to be $0.97 \pm 0.03\,\text{eV}$. Other researchers have reported values in the range of 1.0–0.74 eV (Baur et al., 1989). These data are consistent with our simulations which show this value to be $2E_k = 1.03\,\text{eV}$. Mizubayashi et al. (1995) also reported that the kink pair formation energy decreases with increasing effective stress. While this is consistent with the present simulation results, they did not determine the detailed form of this dependence.

The variation of the dislocation velocity with applied stress is shown in Fig. 7 for temperature in the range $250\,\text{K} \leqslant T \leqslant 600\,\text{K}$. These plots show that velocity increases with applied stress and temperature. The stress dependence is often expressed as a power law

$$v_D = B\left(\frac{\sigma^A}{\tau_P}\right)^m, \tag{11}$$

in the literature (Hirth and Lothe, 1982; Nadgornyi, 1988). The log–log plot of dislocation velocity vs. applied stress (Fig. 7a) yields a near linear behavior, consistent with Eq. (11), although there is clearly some deviation at low stresses. The exponent m and the pre-factor B for Ta (see Table 2) can be expressed as functions of

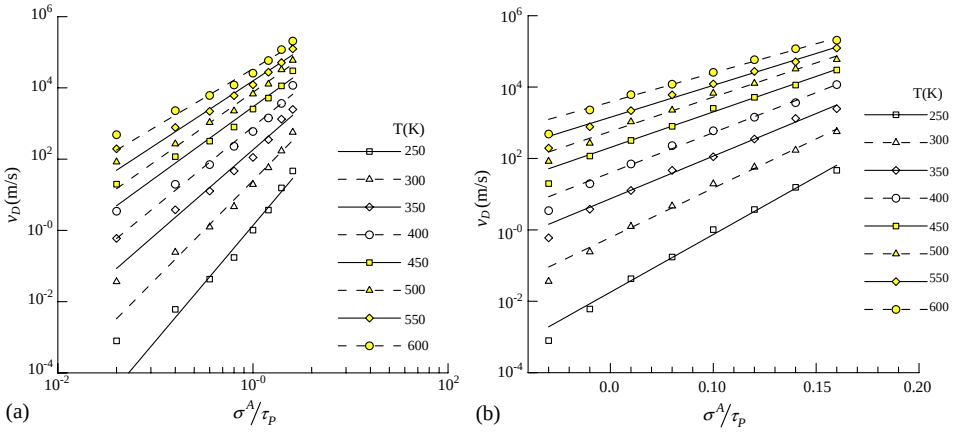

Fig. 7. (a) A log–log plot of the dislocation velocity v_D as a function of the applied stress σ^A at eight different temperatures for pure Ta. The applied stress is expressed as a fraction of the Peierls stress τ_P. The data is expressed as a log–log plot and fit to a power law expression. (b) The same data as in (a) as a log-linear plot and fit to an exponential velocity–stress expression.

Table 2

T (K)	C^{Ta} (m/s)	p^{Ta}	C^{Mo} (m/s)	P^{Mo}
(a) Constants in the power law velocity–stress relation as a function of temperature (Eq. (11)) for Ta (Fig. 7a) and Mo (Fig. 11a)				
250	3.5×10^6	6.51	—	—
300	4.26×10^6	5.54	6.91×10^{-1}	1.69
350	8.73×10^6	4.76	4.50×10^1	1.46
400	1.064×10^7	4.48	2.26×10^2	1.35
450	2.46×10^7	3.91	1.74×10^4	1.22
500	2.74×10^7	3.87	1.10×10^5	1.17
550	6.09×10^7	3.58	4.82×10^5	1.10
600	6.22×10^7	3.24	1.52×10^6	1.04
(b) Constants in the exponential velocity–stress relation as a function of temperature (Eq. (12)) for Ta (Fig. 7b) and Mo (Fig. 11b)				
250	4.324×10^{-4}	74.45	—	—
300	2.549×10^{-2}	63.60	1.687×10^{-5}	19.49
350	4.771×10^{-1}	54.96	2.583×10^{-3}	16.56
400	3.024	51.64	1.055×10^{-1}	15.34
450	2.163×10^1	45.82	2.145	13.09
500	6.289×10^1	44.21	2.053×10^1	12.64
550	1.827×10^2	41.14	1.294×10^2	11.89
600	5.892×10^2	37.51	7.245×10^2	9.85

the temperature:

$$B^{\mathrm{Ta}} = 4.6 \times 10^6 \exp\left(-\frac{0.11\,\mathrm{eV}}{k_{\mathrm{B}}T}\right)\mathrm{m/s}$$
$$m^{\mathrm{Ta}} = 8.1_{(\pm 1.64)} - 8.6_{(\pm 0.24)} \times 10^{-3}(\mathrm{K}^{-1})\,\mathrm{T},$$

where the temperature is expressed in Kelvin. These expressions (and Fig. 7a) demonstrate that the exponent m (slope) decreases with increasing temperature. The velocity is also commonly expressed in the literature through an exponential relation of the form:

$$v_{\mathrm{D}} = C \exp\left(p\,\frac{\sigma^{\mathrm{A}}}{\tau_{\mathrm{P}}}\right). \tag{12}$$

The velocity vs. applied stress data is replotted in Fig. 7b in a manner appropriate for this functional relationship. This figure demonstrates that Eq. (12) provides only a slightly better fit to the velocity–stress data than does the power law expression (Eq. (11)). The parameters C and p in Eq. (12) can be expressed as functions of temperature (see Table 2b) as

$$C^{\mathrm{Ta}} = \gamma_1^{\mathrm{Ta}} \exp\left(-\frac{\gamma_2}{k_{\mathrm{B}}T}\right) = (1.1_{(\pm 0.17)} \times 10^7) \exp\left(-\frac{0.51_{(\pm 0.12)}\,\mathrm{eV}}{k_{\mathrm{B}}T}\right)\mathrm{m/s},$$
$$p^{\mathrm{Ta}} = \delta_1^{\mathrm{Ta}} + \frac{\delta_2^{\mathrm{Ta}}}{k_{\mathrm{B}}T} = 12.6_{(\pm 1.6)} + \frac{1.3_{(\pm 0.23)}\,\mathrm{eV}}{k_{\mathrm{B}}T}.$$

The constant C^{Ta} shows an Arrhenius dependence on temperature with an activation energy that is consistent with that found above (i.e., the energy of a kink E_{k}).

Clearly, the different representations of the velocity–stress–temperature data are not independent. The representations and parameters in Eqs. (8) and (12) suggest that the temperature dependence of the velocity is Arrhenius and that the leading order dependence of the velocity on stress is exponential. Comparison of Eqs. (8) and (12) suggests that $\beta_1 = \gamma_2$ and $\beta_2 = \delta_2$. Examination of the parameters extracted from the fits, ($\beta_1 = 0.49_{(\pm 0.06)}$, $\gamma_2 = 0.51_{(\pm 0.12)}$) and ($\beta_2 = 1.22_{(\pm 0.12)}$, $\delta_2 = 1.31_{(\pm 0.23)}$), demonstrate that the different fits are equivalent. If we expand $\gamma_1^{\mathrm{Ta}} \exp(\delta_1^{\mathrm{Ta}}\sigma^{\mathrm{A}})$ to first order in stress, we should expect that $\alpha_1^{\mathrm{Ta}} = \gamma_1^{\mathrm{Ta}}$ and $\alpha_2^{\mathrm{Ta}} = \gamma_1^{\mathrm{Ta}}\delta_1^{\mathrm{Ta}}$. Comparing with the parameters extracted from the fits ($\alpha_1^{\mathrm{Ta}} = 0.52_{(\pm 0.26)} \times 10^7\,\mathrm{m/s}$, $\gamma_1 = 1.1_{(\pm 0.17)} \times 10^7\,\mathrm{m/s}$) and ($\alpha_2^{\mathrm{Ta}} = 4.0_{(\pm 0.85)} \times 10^8\,\mathrm{m/s}$, $\gamma_1\delta_1 = 1.38_{(\pm 0.03)} \times 10^8\,\mathrm{m/s}$). The fits are less accurate in this case because the expansion of $\exp(\delta_1^{\mathrm{Ta}}\sigma^{\mathrm{A}})$ for small stress is only valid for the lower stresses simulated.

The present results demonstrate that it is possible to adequately fit the screw dislocation velocity in Ta as a function of stress and temperature using Eqs. (8), (11) or (12). The activation energy for migration in pure Ta is consistent with the dislocation velocity being controlled by double kink nucleation.

2.2. Motion of a ⟨1 1 1⟩-oriented screw dislocation in Ta-based alloys

Although analytical predictions of dislocation velocities based upon a kink model description have been proposed and (in some cases) validated, no such predictions are available for alloys. In this section, we extend our kMC method for $(a/2)[1\,\bar{1}\,1]$ screw dislocation in pure bcc Ta to the case of Ta-based alloys. In particular, we examine the effects of short-range (i.e., solute–core) interactions and long-range (i.e., elastic misfit) interactions on dislocation velocity as a function of solute concentration and temperature. The solute atoms are assumed to be immobile at the temperatures of interest (at least on the time scale of the solute size over the dislocation velocity). The parameters in such a study are the solute concentration C_s, the solute–core interaction energy E_b, the variation of lattice parameter a with solute concentration $\delta v = (1/a)(da/dC_s)$, and temperature.

The exact values of solute–core interaction energies and their contribution to the barriers for kink migration are not experimentally known. Several researchers have estimated the heats of segregation of solute at dislocations (Balluffi and Granato, 1979; Granato, 1993; Haasen, 1979, 1983; Takeuchi et al., 1968; Takeuchi, 1969). These values are generally in the range of 0.1–0.75 eV in the refractory bcc metals, with the higher values corresponding to interstitials and the lower to substitutional impurities with nearly the same modulus as the parent (e.g., W in Mo). This sets the approximate magnitude of typical solute–core interactions. Local kink interactions with solute atoms can be either attractive or repulsive, depending on the local core structure and the details of bonding. In the present simulation, we consider the case where an energy E_b must be supplied for a kink to pass through a solute. We consider misfits δv in the range of 0–0.1 which includes such cases as Nb, Mo, and W in Ta (Haasen, 1979, 1983).

Fig. 8 shows the effect of the strength of the solute–core interaction energy on the dislocation velocity as a function of temperature for the case $C_s = 0.1$ and $\delta v = 0.01$ for $\sigma^A = 0.1\,\tau_P$. Even with solute present, the velocity remains an Arrhenius function of temperature (see Eq. (8)). The activation energy $Q^{\text{Ta-alloy}}$ and the pre-factor A (see Eq. (8)) for each dislocation–solute binding energy are as tabulated in Table 3. These data can be fit as

$$A^{\text{Ta-alloy}} = [5.36_{(\pm 0.13)} - 6.03_{(\pm 1.71)} E_b] \times 10^7\ \text{m/s},$$
$$Q^{\text{Ta-alloy}} = 0.4_{(\pm 0.12)}\ \text{eV} + 0.37_{(\pm 0.09)} E_b.$$

The pre-factor $A^{\text{Ta-alloy}}$ decreases and the activation energy $Q^{\text{Ta-alloy}}$ increases linearly with increasing E_b. This leads to an overall decrease in the screw dislocation velocity with increasing dislocation–solute interaction energy. Since the activation energy for the dislocation velocity is dictated by the nucleation of double kinks, the increase in the activation energy for dislocation motion is associated with how the solute increases the double kink nucleation barrier. This is related to the fact that each solute represents repulsive barriers to kink motion and hence double kink expansion. However, since only a fraction of the sites along the dislocation are occupied by solute, the barrier for kink migration varies from place to place. Since

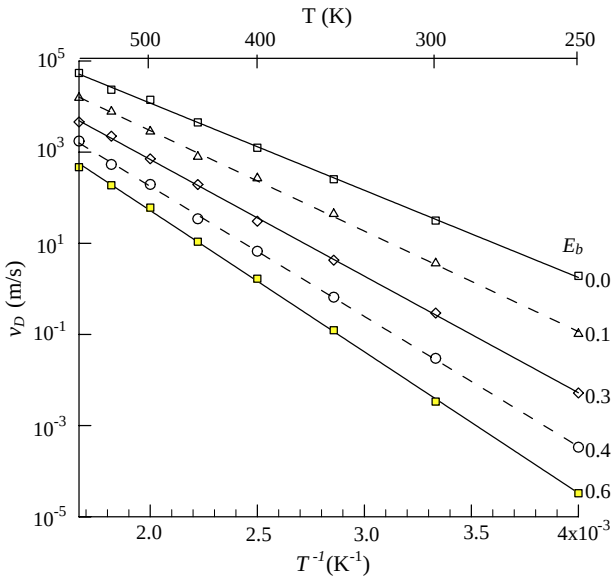

Fig. 8. A semi-log plot of the dislocation velocity v_D as a function of the inverse temperature for five different values of the solute dislocation energy E_b at fixed applied stress ($\sigma^A = 0.1\tau_p$), solute concentration ($C_s = 0.1$) and size misfit ($\delta v = 0.1$). The corresponding temperature is shown in the bar above the plot.

Table 3
Constants in the Arrhenius velocity–temperature relation as a function of solute–core interaction energy E_b (Fig. 8)

E_b (eV)	Q (eV)	$A \times 10^7$ (m/s)
0.00	0.41	5.46
0.15	0.44	4.34
0.30	0.51	3.43
0.45	0.58	2.91
0.60	0.62	1.67

the barriers are not uniform, the coefficient of the solute concentration in the fit to $Q^{\text{Ta-alloy}}$ is less than unity (i.e., 0.37). Note that in addition to increasing the barrier to double kink nucleation, the solute also increases the barrier to the migration of already nucleated kinks migration.

Braithwaite et al. (1971), Wasserbach (1981, 1985), and Briant and Lassila (1999) experimentally investigated the effect of alloying Ta with such alloying elements as W, Mo, Re and Nb. Braithwaite et al. (1971) found that introducing 2.5–15 atomic percent of W, Mo, Re or Nb into Ta leads to a large increase in the flow stress. Although the yield stress cannot be predicted based solely upon single dislocation

simulations, the present results are consistent with an overall increase in yield stress upon alloying. That is, increasing solute concentration produces lower overall kink mobilities and, hence, small screw dislocation velocities. Since the plastic strain rate is proportional to the dislocation velocity, this leads to higher yield stresses, as observed in the experiments. This is consistent with the interpretation of the experimental results suggested by Braithwaite et al. (1971)

In addition to the short-range solute–core interactions, the dislocation motion is also affected by the long-range interactions of the solute and with the elastic field of the dislocation. The stress field of the solute may be calculated using Eq. (7). In order to investigate the effect this interaction has on screw dislocation velocity, we performed a series of simulations in which we vary the size misfit parameter $\delta v = (3/a)(\mathrm{d}a/\mathrm{d}C_s)$. The screw dislocation velocity–temperature relationship is plotted in Fig. 9 for δv in the range from 0 to 0.1. The simulations are performed at an applied stress of 0.1 τ_P and $E_b = 0.15\,\mathrm{eV}$. The parameters Q and A obtained from an Arrhenius fit to the data at different δv are shown in Table 4. We find that linear fits to the data yield

$$Q^{\text{Ta-alloy}} = [0.42_{(\pm 0.1)} + 0.2_{(\pm 0.09)}\delta v]\,\mathrm{eV}$$
$$A^{\text{Ta-alloy}} = [3.6_{(\pm 0.13)} - 28_{(\pm 3.81)}\delta v] \times 10^7\,\mathrm{m/s}.$$

The activation energy Q is only very weakly dependent (apart from statistical fluctuations) upon δv, while the pre-factor A is much more sensitive to this parameter

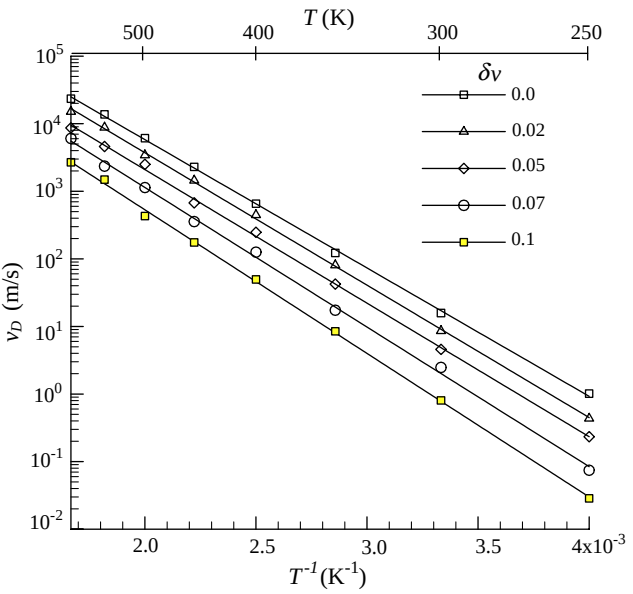

Fig. 9. A semi-log plot of the dislocation velocity v_D as a function of the inverse temperature for five different values of the solute size misfit δv at fixed applied stress ($\sigma^A = 0.1\tau_P$), solute dislocation interaction energy ($E_b = 0.15\,\mathrm{eV}$) and solute concentration ($C_s = 0.01$).

Table 4
Constants in the Arrhenius velocity–temperature relation as a function of solute size misfit δv (Fig. 9)

δv	Q (eV)	$A \times 10^7$ (m/s)
0.000	0.417	3.64
0.025	0.423	3.08
0.050	0.427	1.87
0.075	0.431	1.53
0.100	0.437	0.94

(decreasing with increasing δv). Comparison of the effects of short-range (solute–core) and long-range (elastic) interactions on the dislocation velocities (cf. Figs. 8 and 9 or Tables 3 and 4) clearly shows that the long-range elastic interactions play a much more minor role in decreasing the $(a/2)[1\ \bar{1}\ 1]$ screw dislocation mobility than do the solute–core interactions. This is not surprising, however, because there is no hydrostatic component to the stress field of screw dislocations and the solutes act as centers of dilatation. The small solute misfit effect observed is attributable to the interactions between the solutes and the kinks on the screw dislocations. Recall, that the kinks have edge components and hence produce non-zero hydrostatic stress fields.

We now examine how variations in solute concentration C_s affect screw dislocation velocity in Ta alloys, at fixed $E_b = 0.15\,\text{eV}$ and $\delta v = 0.1$. Fig. 10 shows v_D as a function of the inverse temperature for an applied stress of $0.1\ \tau_P$. Overall, dislocation velocity decreases with increasing solute concentration. The parameters in an Arrhenius fit to this data, $Q^{\text{Ta-alloy}}$ and $A^{\text{Ta-alloy}}$, are shown in Table 5 and can be characterized as linear functions of the solute concentration (see Table 5):

$$Q^{\text{Ta-alloy}} = [0.42_{(\pm 0.06)} + 0.6_{(\pm 0.13)} C_s]\,\text{eV},$$
$$A^{\text{Ta-alloy}} = [4.1_{(\pm 0.3)} - 22_{(\pm 2.4)} C_s] \times 10^7\,\text{m/s}.$$

The variation of the activation energy for dislocation motion $Q^{\text{Ta-alloy}}$ weakly grows with increasing solute concentration, while $A^{\text{Ta-alloy}}$ decreases with increasing solute concentration. The increase in activation energy with increasing concentration can be attributed to the increase in the number of solutes beyond which a double kink must grow in order to reach the critical double kink width, w^*. The decreasing prefactor $A^{\text{Ta-alloy}}$ with increasing solute concentration is likely associated with a net decrease in the mobility of free kinks.

A series of experiments on Ta–W alloys of different compositions by Briant and Lassila (1999) showed that both the yield strength and the rate of work hardening increased with increasing W concentration. They attributed these observations to the effect of solutes on decreasing the mobility of kinks on screw dislocations. This is consistent with the present simulation results.

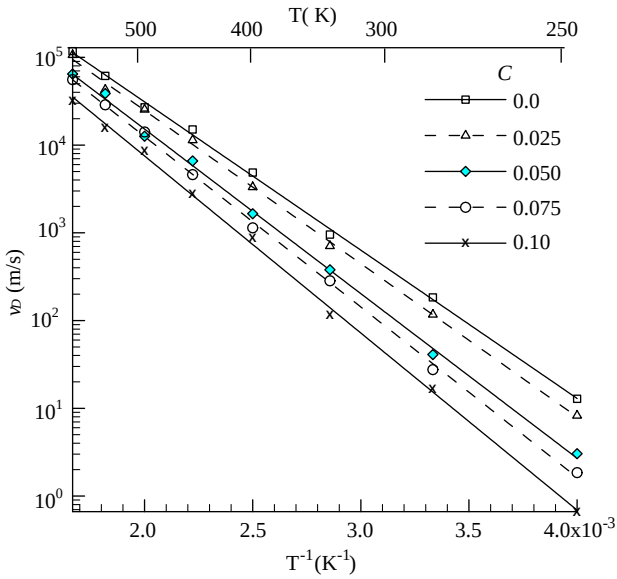

Fig. 10. A semi-log plot of the dislocation velocity v_D as a function of the inverse temperature for five different values of the solute concentration C_s at fixed applied stress ($\sigma^A = 0.1\tau_P$), solute-dislocation interaction energy ($E_b = 0.15\,\text{eV}$) and size misfit ($\delta v = 0.1$).

Table 5
Constants in the Arrhenius velocity–temperature relation as a function of solute concentration C_s (Fig. 10)

C_s	Q (eV)	$A \times 10^7$ (m/s)
0.000	0.42	4.1
0.025	0.44	3.4
0.050	0.45	3.1
0.075	0.47	2.5
0.100	0.48	1.8

3. Discussion

It is interesting to compare the mobilities of the $a/2\ \langle 1\,1\,1\rangle$ screw dislocation in Ta to that in other bcc metals. The most complete set of available data are for Mo, which we determined using the same simulation approach applied here to Ta and reported earlier (Deo et al., 2005). Fig. 11 shows the velocity–stress relationship for the $a/2\ \langle 1\,1\,1\rangle$ screw dislocation in Mo in log–log (Fig. 11a) and log-linear (Fig. 11b) forms (consistent with Eqs. (11) and (12), respectively) for several temperatures. The parameters B^{Mo}, m^{Mo}, C^{Mo} and p^{Mo} (see Eqs. (11) and (12)) are tabulated for different values of the temperature in Table 2. The power-law (Eq. (11), Table 2a)

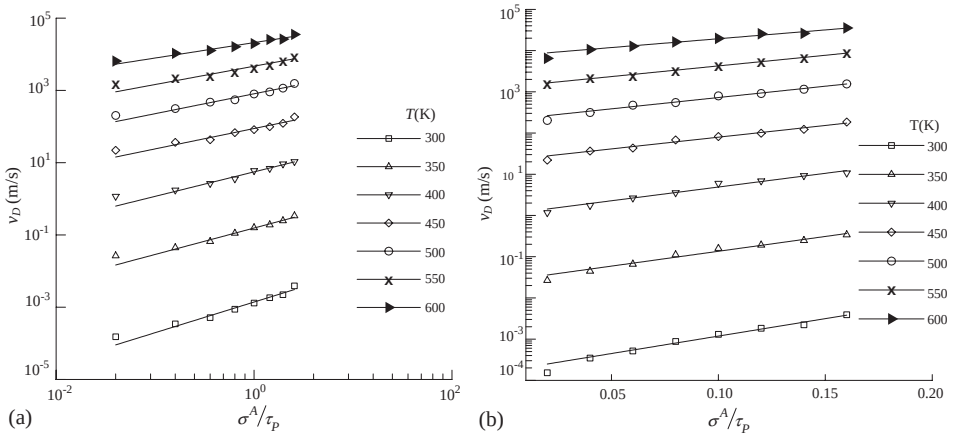

Fig. 11. (a) A log–log plot of the dislocation velocity v_D as a function of the applied stress σ^A at seven different temperatures for pure Mo. The applied stress is expressed as a fraction of the Peierls stress, τ_P. The data is fit to a power law expression. (b) The same data as in (a) as a log-linear plot and fit to an exponential velocity–stress expression.

and exponential (Eq. (12), Table 2b) fit parameters can be expressed as

$$B^{\mathrm{Mo}} = (5.16_{(\pm 1.39)} \times 10^{10}) \exp\left(-\frac{0.91\,\mathrm{eV}}{k_B T}\right) \mathrm{m/s},$$

$$m^{\mathrm{Mo}} = 2.2_{(\pm 0.31)} - 2.05_{(\pm 0.434)} \times 10^{-3}\,(\mathrm{K}^{-1})\mathrm{T},$$

$$C^{\mathrm{Mo}} = (2.8_{(\pm 0.11)} \times 10^{10}) \exp\left(-\frac{0.91_{(\pm 0.12)}\,\mathrm{eV}}{k_B T}\right) \mathrm{m/s},$$

$$p^{\mathrm{Mo}} = 1.6_{(\pm 0.13)} + \frac{0.46_{(\pm 0.05)}\,\mathrm{eV}}{k_B T}.$$

Comparison of the exponents in the power-law fits for Ta and Mo, shows that m^{Ta} is greater than m^{Mo} at all temperatures and that m^{Ta} is more strongly temperature-dependent than m^{Mo}. Examination of the exponents in the exponential fits for Ta and Mo shows that p^{Ta} is much larger than p^{Mo}, which suggests that the dislocation velocity is a stronger function of stress in Ta than in Mo. The stress-independent terms in the activation energy for dislocation motion (the exponents in C^{Ta} and C^{Mo}) correspond to the energy of an isolated single kink, i.e., E_k^{Ta} and E_k^{Mo}, respectively. This is consistent with the screw dislocation velocity being controlled by double kink nucleation in both materials (see Eq. (9)). The activation energy is more strongly stress-dependent in Mo than in Ta (cf. the temperature dependent terms in p^{Ta} and p^{Mo}) after we account for the differences in the Peierls stresses. This ordering (and magnitude) can be understood in terms of the stress dependence of the double kink nucleation barrier (Eqs. (9) and (10)) and accounting for the fact that the shear modulus of Mo is $\sim 70\%$ larger than that of Ta and that the lattice parameters of the

two materials are very similar. Taken together, the Ta and Mo data suggest that screw dislocation velocities in these bcc materials are controlled by double kink nucleation, as represented by Eqs. (9) and (10). These results are also consistent with the experimentally observed temperature dependence of the yield stress.

The simulation results presented above examined the effects of solute misfit, solute–core interactions and solute concentration on dislocation mobility. This model represents the first detailed examination of solute effects in terms of a kink model. This is a reasonable approach, given the success that the kink model has enjoyed in elucidating the behavior of dislocation mobility in pure materials. This approach is capable of including the complexities of solute effects in real alloys; including self-interactions between dislocations, elastic interactions between the solute and dislocation segments, the interactions of solutes with the dislocation core and temperature. Unfortunately, the model is not capable of determining the yield stress or predicting the large scale self-assembly of dislocation microstructures. Rather, the present results provide the key alloy input needed to perform such simulations within the framework of large scale DD simulations. As such, they form the bridge between DD simulations and smaller length and time scale atomistic calculations (e.g., those used to calculate the Peierls stress).

In the present model, solute–dislocation core interactions were assumed to create a repulsive barrier to the motion of kinks. Such barriers may arise when the solute particles interact with the core of the dislocation and affect the planarity of the core and the subsequent motion of the kink. However the exact nature of the solute dislocation interactions is unknown. It may be possible to extract these via atomistic simulation and experimental determinations of solute–core binding energies and double kink formation energies in alloys. This will allow concrete, alloy system-specific predictions of dislocation velocity—applied stress relations.

While the present study focused on solute–core interactions where the kinks were repelled from solute atoms, it is also easy to visualize (and simulate) the opposite case, in which the solute atoms act as kink traps. Alternatively, the solute could segregate to the dislocation core and decrease the Peierls barrier to kink migration or act as heterogeneous sites for double kink nucleation. This could lead to solute-induced softening. If solutes play an important role in DD, than solute transport to dislocations may become important. If the solute makes slip easier and segregation to the dislocation core occurs at high temperature, this could results in increased softening as the temperature is raised upon creation of excess point defects via irradiation (Brunner and Diehl, 1997; Gibala et al., 1970; Pink and Arsenault, 1979). Models for such phenomena remain largely undeveloped. Incorporation of such models in terms of improved unit models for solute–dislocation interactions could easily be incorporated within the kMC framework outlined herein.

In addition to the solute–core interactions, two intrinsic long-range interactions are possible (Haasen, 1979) in alloys. One arises from the difference between the atomic size of the solute and the matrix (considered here) and the other from the influence of the solute on the local elastic modulus of the solvent. The size misfit is usually the dominant long-range interaction. (It is a simple matter to extend this approach to incorporate non-dilatational misfit strains, although it would add some

computational complexity.) Nonetheless, in some substitutional alloys, the size misfit is negligible. Results from our simulation confirm that long-range elastic interactions are less effective in reducing dislocation mobility as compared to short-range solute–core interactions. Just like for size misfit, the modulus effect can be captured in a single parameter $(1/\mu)(\mathrm{d}\mu/\mathrm{d}C_s)$. It would be interesting to compare the differences between the atomic size misfit and modulus effects using the kMC model. The kMC model can be modified to incorporate long-range interactions between the dislocation stress field and a modulus misfit solute. However, doing so makes the elastic problem inhomogeneous, such that simple stress field superposition cannot be used and much more computationally intensive approaches would be required. There are however, simple approximate methods for incorporating the interaction of the inhomogeneous solute with the dislocation (Haasen, 1979).

Several of the parameters employed in the calculation of the double kink nucleation rates and kink diffusivities were obtained from first principles calculations. There is still uncertainty regarding the nature of such calculations for predicting dislocation core properties such as the core energies and structures, Peierls energies and Peierls stress. For example, the energy of well separated kink pair in Ta varies from 0.73 eV (Wang et al., 2002, 2003) to 0.95 eV (Rao and Woodward, 2001; Woodward and Rao, 2001) depending upon the method and pseudopotential employed by the researchers. We use the value determined by Yang et al. (2001a,b) as it is closest to the KPF energy values determined through thermal friction experiments by Mizubayashi et al. (1995) and Baur et al., 1989. Similar uncertainties no doubt exist for such important quantities as the secondary Peierls barrier/stress and the phonon drag coefficient. These uncertainties will produce similar uncertainties in the dislocation mobility in the kMC simulations. Note that some of these uncertainties are magnified by the fact that they appear in exponentials—e.g., the kink pair formation energy.

Atomistic analysis of the core of the $a/2\ \langle 1\,1\,1\rangle$ screw dislocation in bcc metals suggest several possible low energy configurations of the core structure of planar kinks (Bulatov et al., 1997; Duesbery, 1983a,b). Each kink configuration has a unique formation energy. Bulatov et al. (1997) have shown that the kinks of opposite sign may have different mobilities due to asymmetries in the core structures. Such effects are not treated in the model, where we assume the diffusivities of all kinks are the same, except as influenced by the presence or absence of a solute. These effects can be easily incorporated in the model, once appropriate atomistic data becomes available.

That the dislocation mobility is critically dependent on the nature of double kink nucleation further underscores the importance of accurately calculating the double kink nucleation rate. If a double kink is formed with a width smaller than the critical width, the two kinks attract and quickly self-annihilate. The rates of formation and self-annihilation events are so fast that the simulation would normally waste most of its time forming and annihilating sub-critical double kinks. Such a problem was encountered in earlier simulations of dislocation motion (Cai et al., 1999). The solution to this problem employed here was to nucleate a double kink of finite width w_0 which is equal or larger than the critical width w^*. Previous kMC

simulations (Cai et al., 1999; Lin and Chrzan, 1999) have made ad-hoc assumptions regarding the calculation of the double kink nucleation rate. Given the importance of double kink nucleation within the kink model, it is necessary to ensure that the calculation of the rate at which supercritical double kinks forms is consistent with the real time spent forming and self-annihilating sub-critical double kinks. By treating double kink nucleation as a 1-d random walker in double kink width space, we were able to obtain a distribution of double kink nucleation times from a first passage time analysis (Deo and Srolovitz, 2002). However, the double kink nucleation rate is also subject to the same uncertainties as for kink migration, since kink migration is an intrinsic part of double kink nucleation.

4. Conclusion

We have applied a kMC algorithm to simulate the motion of $a\ 1/2\langle 1\,1\,1\rangle$-oriented screw dislocation on a $\{0\,1\,1\}$-slip plane in pure bcc Ta and Ta-based alloys. Simulations were performed to determine dislocation velocity as a function of stress, temperature and solute concentration. The dislocation velocity exhibited an Arrhenius dependence on temperature with an activation energy that is strongly dependent on the double kink nucleation energy (and hence the kink formation energy and the local stress). These results are consistent with some existing analytical predictions of the dependence of the dislocation velocity on these parameters. In the case of Ta, the activation energy for dislocation motion is controlled by the double kink nucleation rate. Solute additions reduced the dislocation velocity. The dominant solute–dislocation interaction is that associated with the short-range solute–core interactions rather than the long-range interactions between the elastic fields of the solute and the dislocations. Although the present model is very general and can be used to study dislocation motion in a wide range of alloys, its accuracy is mainly limited by uncertainty in several fundamental dislocation and solute parameters (e.g., single kink energy, secondary Peierls barrier to kink migration, single kink mobility, solute–dislocation core interaction energies). These parameters can all be obtained from first principles calculations and/or molecular dynamics simulations. The present method provides the critical link between atomistic calculations of these fundamental parameters and dislocation dynamics simulations that track the evolution of a large number of dislocations. Incorporation of the kMC results extends such DD to the common case of metallic alloys, rather than simply pure metals.

References

Balluffi, R., Granato, A., 1979. Dislocations, vacancies and interstitials. In: Nabarro, Dislocations in Solids, vol. IV. pp. 1–133.

Basinski, Z.S., et al., 1970. Screw dislocation in a model sodium lattice. Philos. Mag. 21 (174), 1201–1221.

Baur, J., et al., 1989. The dislocation—internal friction peak gamma in tantalum. Acta Metall. 37 (4), 1159–1166.

Bortz, A., et al., 1975. New algorithm for Monte-Carlo simulation of Ising spin systems. J. Comput. Phys. 17 (1), 10–18.
Braithwaite, A.A., et al., 1971. Solid solution hardening in tantalum alloys. Z. Metall. 62 (8), 596–600.
Briant, C.L., Lassila, D.H., 1999. The effect of tungsten an the mechanical properties of tantalum. J. Eng. Mater. Technol.-Trans. ASME 121 (2), 172–177.
Brunner, D., Diehl, J., 1997. The effect of atomic lattice defects on the softening phenomena of high-purity alpha -iron. Physica Status Solidi A, Third International Conference on Ultra-High-Purity Base Metals, (UHPM-96), 160(2), pp. 355–372.
Bulatov, V., et al., 1997. Kink asymmetry and multiplicity in dislocation cores. Phys. Rev. Lett. 79 (25), 5042–5045.
Bulatov, V., et al., 1998. Connecting atomistic and mesoscale simulations of crystal plasticity. Nature 391 (6668), 669–672.
Bulatov, V., et al., 2001. Crystal plasticity from dislocation dynamics. MRS Bull. 26 (3), 191–195.
Cai, W., et al., 1999. Kinetic Monte Carlo method for dislocation glide in silicon. J. Comput.-Aided Mater Design 6 (2–3), 175–183.
Cai, W., et al., 2001. Kinetic Monte Carlo modeling of dislocation motion in bcc metals. Mater. Sci. Eng. A 309, 270–273.
Cai, W., et al., 2002. Kinetic Monte Carlo approach to modeling dislocation mobility. Comput. Mater. Sci. 23, 124.
Cuitino, A., Ortiz, M., 1993. Computational modelling of single crystals. Modelling Simulation Mater. Sci. Eng. 1 (3), 225–263.
Deo, C.S., Srolovitz, D.J., 2002. First passage time Markov chain analysis of rare events for kinetic Monte Carlo: Double kink nucleation during dislocation glide. Modelling Simulation Mater. Sci. Eng. 10 (5), 581–596.
Deo, C.S., et al., 2005. Kinetic Monte Carlo simulations of dislocation mobility in bcc alloys. Phys. Rev. B (Condensed Matter and Materials Physics), accepted for publication.
Duesbery, M., 1983a. On kinked screw dislocations in the bcc lattice. I. The structure and Peierls stress of isolated kinks. Acta Metall. 31 (10), 1747–1758.
Duesbery, M., 1983b. On kinked screw dislocations in the bcc lattice. II. Kink energies and double kinks. Acta Metall. 31 (10), 1759–1770.
Duesbery, M.S., Vitek, V., 1998. Plastic anisotropy in bcc transition metals. Acta Mater. 46 (5), 1481–1492.
Duesbery, M.S., et al., 1973. Effect of shear-stress on screw dislocation core structure in body-centered cubic lattices 35. Proc. Roy. Soc. London Series A—Math. Phys. Eng. Sci. 332 (1588), 85–111.
Eshelby, J., 1962. Interaction of kinks and elastic waves. Proc. Roy. Soc. London Series A-Math. Phys. Sci. 266 (1325), 222–246.
Gibala, R., et al., 1970. Dislocation relaxation in single crystals of bcc metals. J. Phys. Chem. Solids 31 (8), 1889–1899.
Gillespie, D.T., 1992. Markov processes: An Introduction for Physical Scientists. Academic Press, Boston, MA.
Granato, A., 1993. Inertial effects of dislocations. Materials Science Forum 119/121, 767–770.
Haasen, P., 1979. Solution hardening in f.c.c. metals. In: Nabarro (Ed.), Dislocations in solids, vol. IV. Dislocations in metallurgy, p. 155–189.
Haasen, P., 1983. Mechanical properties of solid solutions and intermetallic compounds. In: Cahn, Haasen (Eds.), Physical metallurgy, Third revised and enlarged edition, vol. 2, pp. 1341–1409.
Hirsch, P.B., 1959. Observations of dislocations in metals by transmission electron microscopy. J. Inst. Metals 87 (12), 406–418.
Hirsch, P.B., et al., 1957. Electron microscope observations of dislocations in metals. Acta Crystallogr. 10 (12), 823–824.
Hirsch, P.B., et al., 1960. A kinematical theory of diffraction contrast of electron transmission microscope images of dislocations and other defects. Philos. Trans. Roy. Soc. London Series A-Math. Phy. Sci. 252 (1017), 499–529.
Hirth, J.P., Lothe, J., 1982. Theory of Dislocations. Wiley, New York.
Ismail-Beigi, S., Arias, T.A., 2000. Ab initio study of screw dislocations in Mo and Ta: A new picture of plasticity in bcc transition metals. Phys. Rev. Lett. 84 (7), 1499–1502.

Lin, K., Chrzan, D.C., 1999. Kinetic Monte Carlo simulation of dislocation dynamics. Phys. Rev. B 60 (6), 3799–3805.

Mizubayashi, H., et al., 1995. Anelastic study of screw-dislocation motion in high-purity tantalum. Acta Metall. Mater. 43 (1), 269–276.

Nadgornyi, E., 1988. Dislocation Dynamics and Mechanical Properties of Crystals, vol. 31. Pergamon Press, Oxford, New York.

Ortiz, M., 1999. Plastic yielding as a phase transition. Trans. ASME J. Appl. Mech. 66 (2), 289–298.

Pink, E., Arsenault, R., 1979. Low-temperature softening in body-centered cubic alloys. Prog. Mater. Sci. 24 (1), 1–50.

Rao, S., Woodward, C., 2001. Atomistic simulations of $(a/2)\ \langle 1\,1\,1\rangle$ screw dislocations in bcc Mo using a modified generalized pseudopotential theory potential. Philos. Mag. A (Physics of Condensed Matter: Structure, Defects and Mechanical Properties) 81 (5), 1317–1327.

Scarle, S., et al., 2001. Kinetic Monte Carlo study of dislocation motion in silicon: Soliton model and hydrogen enhanced glide. PHYSICA B, 21st International Conference on Defects in Semiconductors 308, pp. 493–496.

Seeger, A., 1981. The kink picture of dislocation mobility and dislocation-point-defect interactions. J. Phys. 42 (C5), 201–228.

Seeger, A., Sestak, B., 1971. Microstrain and dislocation relaxations in bcc metals. Scr. Metall. 5 (10), 875–882.

Stainier, L., et al., 2003. Multiscale modelling of hardening in bcc crystal plasticity. J. Phys. IV (Proceedings), 6th European Mechanics of Materials Conference on Non-Linear Mechanics of Anisotropic Materials. EUROMECH-MECAMAT'2002, 9–12 September 2002, Liege, Belgium, vol. 105, 157–164.

Takeuchi, S., 1969. Solid-solution strengthening in single crystals of iron alloys. J. Phys. Soc. Japan 27 (4), 929–940.

Takeuchi, S., et al., 1968. Solid-solution strengthening in iron alloys. Trans. Japan Inst. Metals 9, 715–719.

Tang, M., et al., 1998. Dislocation mobility and the mechanical response of bcc single crystals: a mesoscopic approach. Acta Mater. 46 (9), 3221–3235.

Tang, M., et al., 1999. Simulation and modelling of forest hardening in body centre cubic crystals at low temperature. Modelling Simulation Mater. Sci. Eng. Gilles Canova Memorial Symposium on Multi-scale Modelling of Mechanical Properties of Materials 7 (5), 893–908.

Vitek, V., 1976. Computer-simulation of screw dislocation-motion in bcc metals under effect of external shear and uniaxial stresses. Proc. Roy. Soc. London Series A 352 (1668), 109–124.

Vitek, V., 1985. Dislocation core effects in plastic-deformation. Trans. Indian Inst. Metals 38 (6), 510–518.

Vitek, V., Taylor, G., 1974. Anomalous slip in bcc crystals observed in computer-simulation of screw dislocation-motion-comment. Scr. Metall. 8 (11), 1283–1285.

Wang, G., et al., 2001. Molecular dynamics simulations of a $1/2a$ $(1\,1\,1)$ screw dislocation in Ta. Mater. Sci. Eng. A 309, 133–137.

Wang, G.F., et al., 2002. Kinks in the $a/2\ \langle 1\,1\,1\rangle$ screw dislocation in Ta. J. Comput-Aided Mater. Des. 8 (2–3), 117–125.

Wang, G.F., et al., 2003. Atomistic simulations of kinks in $1/2a\ \langle 2\,2\,1\,1\,1\rangle$ screw dislocations in bcc tantalum. Phys. Rev. B 68 (22), 224101.

Wasserbach, W., 1981. Anomalous slip in tantalum single-crystals after tensile deformation at 77-K. Z. Metal. 72 (6), 445–450.

Wasserbach, W., 1985. Anomalous slip in high-purity tantalum single-crystals after tensile deformation at 77-K. Philos. Mag. A 51 (4), 619–628.

Woodward, C., Rao, S.I., 2001. Ab-initio simulation of isolated screw dislocations in bcc Mo and Ta. Philos. Mag. A 81 (5), 1305–1316.

Yang, L.H., Moriarty, J.A., 2001. Kink-pair mechanisms for $a/2\ \langle 1\,1\,1\rangle$ screw dislocation motion in bcc tantalum. Mater. Sci. Eng. A 319, 124–129.

Yang, L.H., et al., 2001a. Accurate atomistic simulation of $(a/2)\ \langle 1\,1\,1\rangle$ screw dislocations and other defects in bcc tantalum. Philos. Mag. A 81 (5), 1355–1385.

Yang, L.H., et al., 2001b. Atomistic simulation of pressure-dependent screw dislocation properties in bcc tantalum. Mater. Sci. Eng. A 309, 102–107.